JACC: BASIC TO TRANSLATIONAL SCIENCE VOL. 6, NO. 4, 2021

CLINICAL RESEARCH

SARS-CoV-2 Infects Human Engineered Heart Tissues and Models COVID-19 Myocarditis

Adam L. Bailey, MD, PhD,[a,*] Oleksandr Dmytrenko, BA,[b,*] Lina Greenberg, PhD,[c,*] Andrea L. Bredemeyer, PhD,[b] Pan Ma, PhD,[b] Jing Liu, MS,[b] Vinay Penna, BS,[b] Emma S. Winkler, BS,[a] Sanja Sviben, PhD,[d] Erin Brooks, MD,[e] Ajith P. Nair, MD,[f] Kent A. Heck, MD,[g] Aniket S. Rali, MD,[h] Leo Simpson, MD,[f] Mehrdad Saririan, MD,[i] Dan Hobohm, MD,[i] W. Tom Stump, PhD,[c] James A. Fitzpatrick, PhD,[d,j] Xuping Xie, PhD,[k] Xianwen Zhang, PhD,[k] Pei-Yong Shi, PhD,[k] J. Travis Hinson, MD,[l,m] Weng-Tein Gi, MD, MSc,[n] Constanze Schmidt, MD,[n] Florian Leuschner, MD,[n] Chieh-Yu Lin, MD, PhD,[a,†] Michael S. Diamond, MD, PhD,[a,b,o,†] Michael J. Greenberg, PhD,[c,†] Kory J. Lavine, MD, PhD[a,b,p,†]

VISUAL ABSTRACT

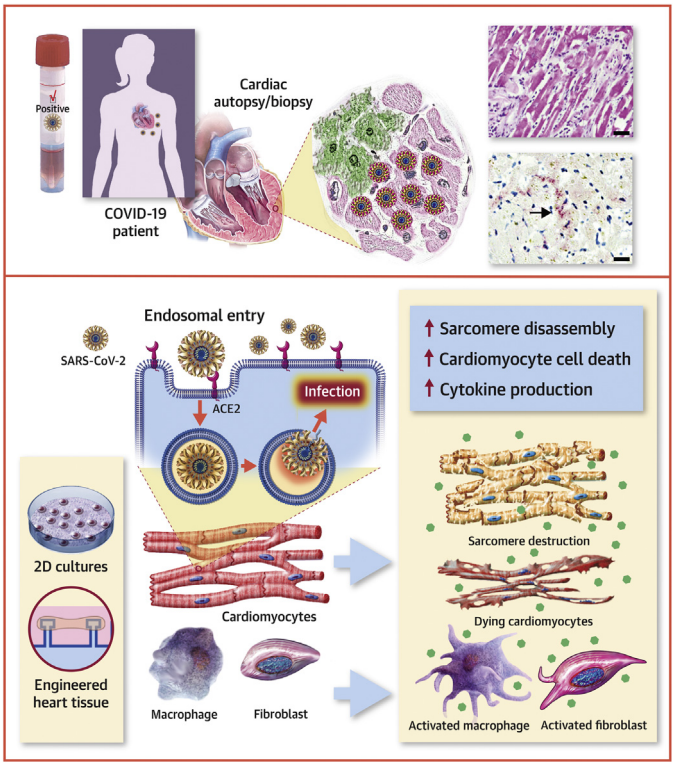

Bailey, A.L. et al. J Am Coll Cardiol Basic Trans Science. 2021;6(4):331–45.

HIGHLIGHTS

- SARS-CoV-2 directly infects cardiomyocytes in patients with COVID-19 myocarditis and does not infect cardiac macrophages, fibroblasts, or endothelial cells.
- COVID-19 myocarditis is characterized by a myeloid-rich inflammatory infiltrate.
- SARS-CoV-2 infects cardiomyocytes through an ACE2 and endosomal cysteine protease dependent pathway.
- Infection of hPSC-derived cardiomyocytes and engineered heart tissues show that cytokine production, sarcomere disassembly, and cell death were a direct consequence of cardiomyocyte infection.
- SARS-CoV-2 reduces cardiomyocyte contractility through sarcomere breakdown and cardiomyocyte cell death.

From the [a]Department of Pathology and Immunology, Washington University School of Medicine, St. Louis, Missouri, USA; [b]Cardiovascular Division, Department of Medicine, Washington University School of Medicine, St. Louis, Missouri, USA; [c]Department of Biochemistry and Molecular Biophysics, Washington University School of Medicine, St. Louis, Missouri, USA; [d]Washington University Center for Cellular Imaging, Washington University School of Medicine, St. Louis, Missouri, USA; [e]Department of Pathology & Laboratory Medicine, University of Wisconsin Hospital and Clinics, Madison, Wisconsin, USA; [f]Department of

ISSN 2452-302X https://doi.org/10.1016/j.jacbts.2021.01.002

ABBREVIATIONS AND ACRONYMS

ACE2 = angiotensin converting enzyme 2

COVID-19 = coronavirus disease-2019

EHT = engineered heart tissues

hPSC = human pluripotent stem cell(s)

LV = left ventricle

SARS-CoV-2 = severe acute respiratory syndrome-coronavirus-2

SUMMARY

There is ongoing debate as to whether cardiac complications of coronavirus disease-2019 (COVID-19) result from myocardial viral infection or are secondary to systemic inflammation and/or thrombosis. We provide evidence that cardiomyocytes are infected in patients with COVID-19 myocarditis and are susceptible to severe acute respiratory syndrome coronavirus 2. We establish an engineered heart tissue model of COVID-19 myocardial pathology, define mechanisms of viral pathogenesis, and demonstrate that cardiomyocyte severe acute respiratory syndrome coronavirus 2 infection results in contractile deficits, cytokine production, sarcomere disassembly, and cell death. These findings implicate direct infection of cardiomyocytes in the pathogenesis of COVID-19 myocardial pathology and provides a model system to study this emerging disease. (J Am Coll Cardiol Basic Trans Science 2021;6:331–45)

Severe acute respiratory syndrome-coronavirus-2 (SARS-CoV-2) is the cause of the ongoing coronavirus disease-2019 (COVID-19) pandemic. Epidemiological studies have identified pre-existing cardiovascular disease as a risk factor for the development of severe COVID-19 and mortality [reviewed in Madjid et al. (1)]. Cardiovascular manifestations of COVID-19 include elevated troponin, reduced left ventricular (LV) systolic function, and arrhythmias. Cardiac complications occur in 20% to 44% of hospitalized patients, and constitute an independent risk factor for COVID-19 mortality (1–4). Cardiac magnetic resonance imaging studies have suggested that persistent myocardial injury may be more common than appreciated and occurs in less severe forms of COVID-19 (5–7). The mechanistic basis by which SARS-CoV-2 results in cardiac dysfunction remains obscure and it is unclear whether these effects are a result of myocardial infection or a systemic inflammatory response to extracardiac infection (8).

Investigation of the cardiac manifestations of COVID-19 has remained challenging. Rigorous analyses of cardiac tissue obtained from affected patients are lacking. Furthermore, there are few animal models to study cardiovascular complications observed in SARS-CoV-2-infected humans (9). The most commonly used laboratory animal model, the mouse, is not susceptible to SARS-CoV-2 infection due to poor affinity of the viral spike protein for murine angiotensin converting enzyme 2 (ACE2). Transgenic mice that express human ACE2 under the control of the cytokeratin 18 promotor do not recapitulate ACE2 expression within the human cardiovascular system (10–12). Therefore, there is a critical need to develop robust model systems that enable the investigation of the cardiovascular complications of COVID-19.

We used human myocardial specimens and devised an engineered heart tissue (EHT) model of COVID-19 myocarditis to test the hypothesis that SARS-CoV-2 promotes cardiac pathology by infecting cardiomyocytes and activating local immune responses. EHT provide unique advantages as model systems for studying COVID-19 cardiac pathology because they generate contractile force, display electrical coupling, promote maturation of human

Medicine, Baylor College of Medicine, Houston, Texas, USA; [g]Department of Pathology, Baylor College of Medicine, Houston, Texas, USA; [h]Department of Medicine, Vanderbilt University, Nashville, Tennessee, USA; [i]Valleywise Health/Creighton University, Phoenix, Arizona, USA; [j]Departments of Neuroscience, Cell Biology & Physiology, and Biomedical Engineering, Washington University School of Medicine, St. Louis, Missouri, USA; [k]Department of Biochemistry and Molecular Biology, University of Texas Medical Branch, Galveston, Texas, USA; [l]Departments of Cardiology, Genetics and Genome Sciences, UConn Health, Farmington, Connecticut, USA; [m]The Jackson Laboratory for Genomic Medicine, Farmington, Connecticut, USA; [n]Department of Internal Medicine III, University Hospital Heidelberg, University of Heidelberg, Heidelberg, Germany; [o]Department of Molecular Microbiology, Washington University School of Medicine, St. Louis, Missouri, USA; and the [p]Department of Developmental Biology, Washington University School of Medicine, St. Louis, Missouri, USA. Michael R. Bristow, MD, PhD, served as Guest Editor-in-Chief for this paper. *Drs. Bailey and L. Greenberg, and Mr. Dmytrenko contributed equally to this work and are joint first authors. †Drs. Lin, Diamond, M. J. Greenberg, and Lavine contributed equally to this work and are joint senior authors.

The authors attest they are in compliance with human studies committees and animal welfare regulations of the authors' institutions and Food and Drug Administration guidelines, including patient consent where appropriate. For more information, visit the Author Center.

Manuscript received December 3, 2020; revised manuscript received January 5, 2021, accepted January 5, 2021.

FIGURE 1 **Specimens From Patients With Severe COVID-19 Myocarditis Show Evidence of SARS-CoV-2 Cardiomyocyte Infection**

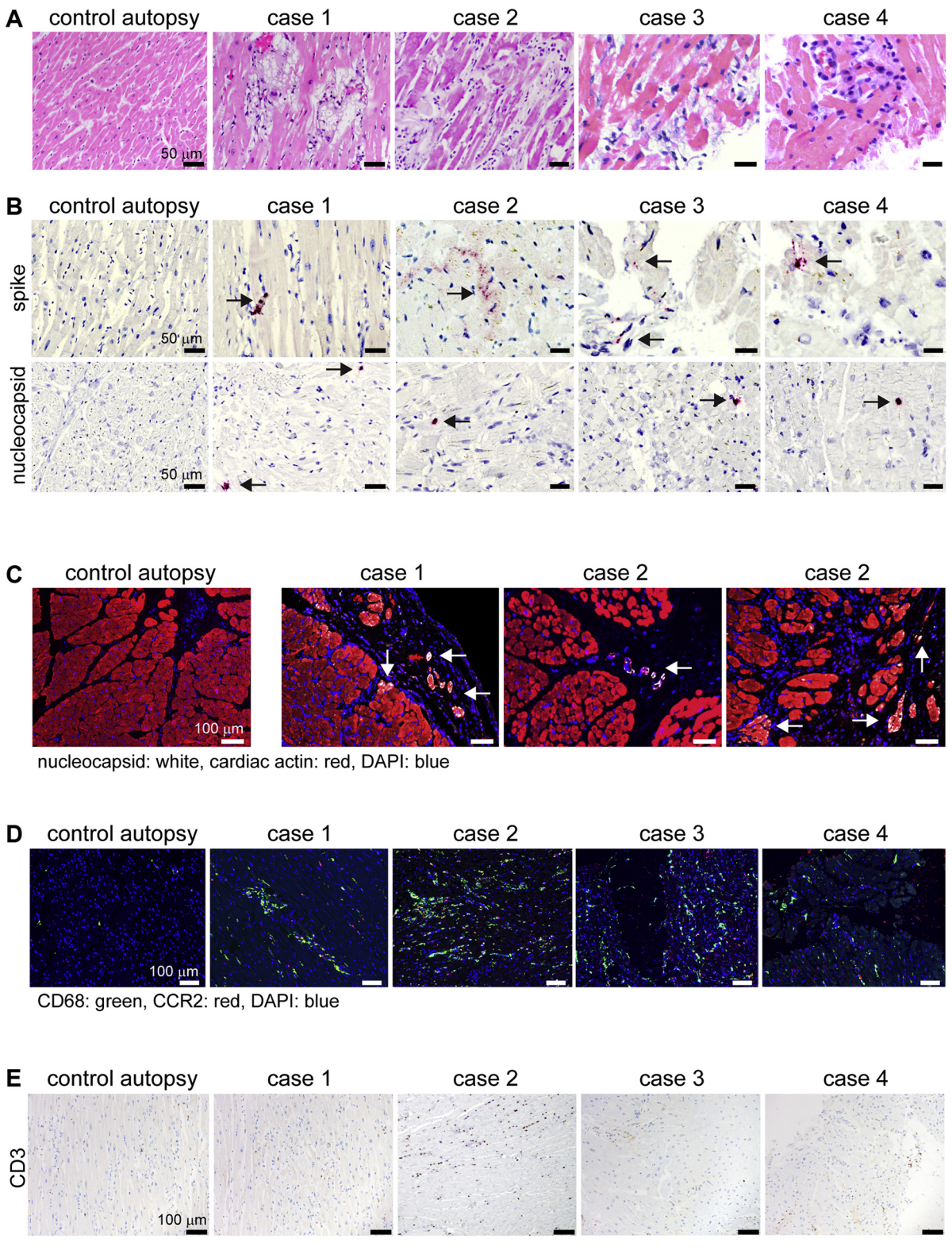

Continued on the next page

pluripotent stem cell (hPSC)-derived cardiomyocytes, and have cellular organization that mimics myocardial tissue (12–14). These studies show that cardiomyocytes are a target of SARS-CoV-2, link cardiomyocyte infection to disease pathogenesis, and establish EHT as an experimentally tractable model of COVID-19 myocardial pathology.

METHODS

A detailed methods section, including Supplemental Tables 1 and 2, is in the Supplemental Appendix.

BIOSAFETY. This study was approved by the IRB of Washington University Medical School. All work with infectious SARS-CoV-2 was performed in a biosafety level 3 facility by personnel equipped with a powered air purifying respirator.

VIRUSES. The 2019n-CoV/USA_WA1/2019 isolate of SARS-CoV-2 was obtained from the United States Centers for Disease Control. Information on the NeonGreen SARS-CoV-2-NeonGreen virus was discussed in Xie et al. (13). All infections were performed at a multiplicity of infection (MOI) of 0.1.

hPSC CARDIOMYOCYTE DIFFERENTIATION AND EHTs. Stem cells were differentiated by temporal manipulation of Wnt signaling and metabolic selection. EHTs were assembled in polydimethylsiloxane (PDMS) casting molds (EHT Technologies, Hamburg, Germany) from hPSC-derived cardiomyocytes, fibroblasts, and/or macrophages. EHTs were inoculated with SARS-CoV-2 at least 7 days after tissue seeding.

STATISTICAL ANALYSIS. Statistical tests were chosen based on accepted standards. The Kolmogorov-Smirnov test was used to test for normality. Parametric (Student t test, analysis of variance [ANOVA]) and nonparametric (Mann-Whitney test) statistical methods were used when appropriate. Statistical significance was assigned when p values were <0.05 using Prism Version 8 (GraphPad, San Diego, California). Specific tests are indicated in the figure legends. Mean values and median values are displayed for parametric tests and nonparametric tests, respectively.

RESULTS

EVIDENCE OF CARDIOMYOCYTE INFECTION IN SEVERE COVID-19 MYOCARDITIS. The pathology of COVID-19 myocarditis remains poorly understood. We obtained autopsy and endomyocardial biopsy specimens from 4 subjects with SARS-CoV-2 infection and clinical diagnoses of myocarditis. Myocardial injury and LV systolic dysfunction were present in each case (Supplemental Table 3). Coronary angiography showed no evidence of luminal stenosis or thrombosis. The presence of SARS-CoV-2 RNA from nasopharyngeal samples was confirmed by clinical polymerase chain reaction (PCR) testing.

Postmortem microscopic examination of the LV myocardium showed areas of cardiomyocyte necrosis and degenerative vacuolization of cardiomyocyte cytoplasm accompanied by a mononuclear cell infiltrate (**Figure 1A**). These changes were distinct from postmortem autolytic changes. Examination of the coronary arteries from COVID-19 myocarditis autopsy cases showed nonobstructive mild atherosclerotic changes, consistent with angiogram findings. There was no evidence of microvascular injury or thromboembolic events. Autopsy heart samples from subjects with metastatic carcinoma and an inherited neurodegenerative disease with similar tissue procurement times were included as negative controls.

SARS-CoV-2 spike and nucleocapsid RNA was detected within the myocardium of each COVID-19 myocarditis subject. Viral transcripts were located in cytoplasmic and perinuclear locations within cells that were morphologically consistent with cardiomyocytes (**Figure 1B**). Viral transcripts were also present lung airway epithelial cells and rare myocardial adipocytes and pericytes (Supplemental Figure 1). Immunostaining for the SARS-CoV-2 nucleocapsid protein showed presence of viral protein in cardiomyocytes (**Figure 1C**). The immune cell infiltrate was characterized by accumulation of an

FIGURE 1 Continued

(A) Hematoxylin and eosin staining of cardiac autopsy (anterior left ventricular wall) and biopsy samples (right ventricular septum) from subjects without coronavirus disease-2019 (COVID-19) (control case) and patients with severe COVID-19 myocarditis (case 1-4). **(B)** In situ hybridization for severe acute respiratory syndrome-coronavirus-2 (SARS-CoV-2) spike and nucleocapsid RNA **(red).** Hematoxylin: blue. The **arrows** denote viral RNA staining in cells with cardiomyocyte morphology. **(C)** Immunostaining of control and COVID-19 myocarditis cardiac autopsy tissue for SARS-CoV-2 nucleocapsid **(white)** and cardiac actin **(red).** DAPI: **blue**. The **arrows** denote nucleocapsid staining in cardiomyocytes. **(D)** Immunostaining of control and COVID-19 myocarditis specimens for CD68 **(green)** and CCR2 **(red).** DAPI: **blue**. **(E)** Immunostaining of control and COVID-19 myocarditis tissue for CD3 **(brown).** Hematoxylin: blue. DAPI = 4′,6-diamidino-2-phenylindole.

FIGURE 2 **SARS-CoV-2 Infects Cardiomyocytes**

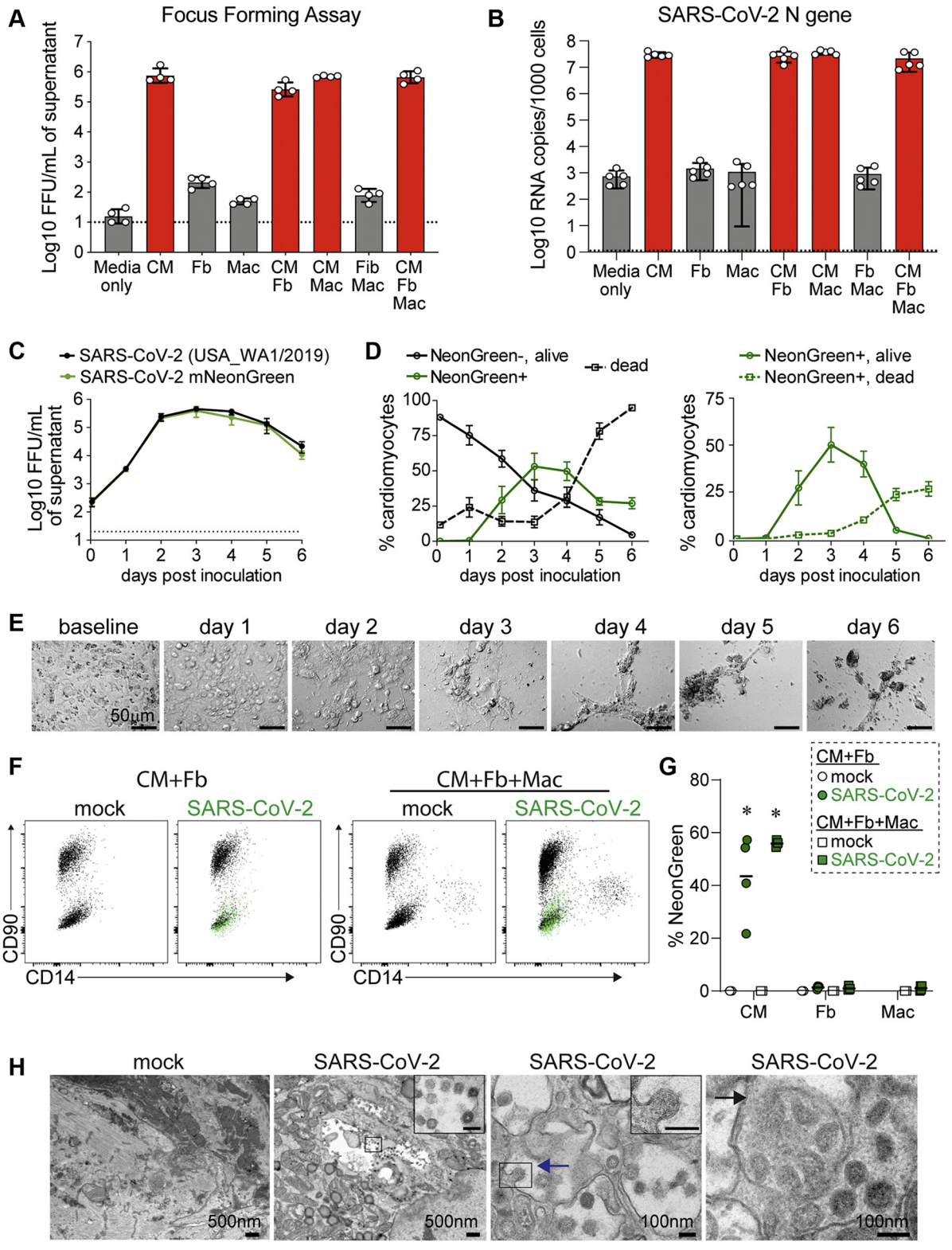

Continued on the next page

admixture of $CCR2^-$ and $CCR2^+$ macrophages (**Figure 1D**). Minimal T-cell infiltration was noted (**Figure 1E**). Macrophage abundance was highest in areas of cardiomyocyte injury as depicted by complement deposition (C4d staining, Spearman $r = 0.86$, $p = 0.0005$), a pathological marker of cardiomyocyte cell death (14-16) (Supplemental Figure 1). These observations suggest that SARS-CoV-2 can infect the human heart and may contribute to cardiomyocyte cell death and myocardial inflammation.

SARS-CoV-2 TROPISM IN THE HUMAN HEART. ACE2 serves as a cell-surface receptor for SARS-CoV-2 through interactions with the spike protein (17,18). Consistent with prior reports, we detected ACE2 mRNA expression in the human heart across the spectrum of age increasing in heart failure (19,20). ACE2 mRNA was expressed in cardiomyocytes with significant variation in ACE2 protein expression between individual cardiomyocytes. hPSC-derived cardiomyocytes and EHTs expressed ACE2 mRNA and protein (Supplemental Figures 2 and 3).

To determine the susceptibility of different myocardial cell types to SARS-CoV-2 infection, we inoculated combinations of hPSC-derived cardiomyocytes, fibroblasts, and macrophages with wild-type SARS-CoV-2 (USA_WA1/2019). We analyzed tissue culture supernatants for production of infectious virus and measured intracellular viral RNA transcript levels at 3 days post-inoculation. These assays revealed production of infectious virus (**Figure 2A**) and viral RNA (**Figure 2B**) in cultures that contained hPSC-derived cardiomyocytes. Cultures lacking hPSC-derived cardiomyocytes contained viral loads that were equivalent to media-only controls.

To verify cardiomyocyte selective tropism, we inoculated human cardiac stromal populations with a recombinant SARS-CoV-2 clone containing a NeonGreen fluorescent reporter (SARS-CoV-2-NeonGreen) (13). NeonGreen is expressed from a viral subgenomic RNA, indicative of active viral replication. Primary human cardiac fibroblasts, endothelial cells, and macrophages were not permissive to SARS-CoV-2 infection (Supplemental Figures 3 to 5). hPSC-derived endothelial cells and cardiac fibroblasts were also not susceptible to infection. In contrast, 2 independent lines of hPSC-derived cardiomyocytes were permissive to SARS-CoV-2 infection. Undifferentiated hPSC lines did not show evidence of infection (Supplemental Figure 5). hPSC-derived cardiomyocyte infection showed rapid production of infectious virus with peak titers on day 3 post-inoculation (**Figure 2C**).

We examined the relationship between viral replication and cell death. NeonGreen-positive cardiomyocytes peaked at day 3 post-inoculation. hPSC-derived cardiomyocyte cell death was observed beginning 4 to 5 days post-inoculation (**Figure 2D**) indicating that viral infection precedes cell death. SARS-CoV-2-infected cardiomyocytes displayed characteristics of cytopathic effect, cellular rounding, clumping, and syncytium formation. Distortion of cellular morphology was evident by day 4 post-inoculation and cultures contained largely dead cells and debris by days 5 to 6 post-inoculation (**Figure 2E**).

To examine whether cardiomyocytes are a target of SARS-CoV-2 in a simulated cardiac environment, we infected 2-dimensional tissues assembled with hPSC-derived cardiomyocytes (80%), fibroblasts (10%), and macrophages (10%) with SARS-CoV-2-NeonGreen. Flow cytometry performed 3 days following infection revealed NeonGreen expression only in

FIGURE 2 Continued

(A) Focus-forming assay measuring production of infectious virus from human pluripotent stem cell (hPSC)–derived cardiomyocytes (CM), fibroblasts (Fb), and macrophages (Mac) inoculated with SARS-CoV-2 (multiplicity of infection [MOI], 0.1). Media only denotes wells that contain no cells. Assays were performed 3 days following inoculation. **Dashed line** indicates limit of assay detection. **(B)** Quantitative real-time polymerase chain reaction (RT-PCR) showing viral N-gene copies in cultures containing CM, Fb, and Macs inoculated with SARS-CoV-2 (MOI 0.1). RNA was collected 3 days post-inoculation ($n = 5$ per group). **(C)** Focus-forming assay measuring infectious SARS-CoV-2 (**black line** indicates wild-type; **green line** indicates NeonGreen) in supernatant of hPSC-derived cardiomyocytes over time following inoculation (MOI 0.1). A **dashed line** indicates the limit of detection ($n = 4$ per group). **(D)** Two-dimensional cultures of hPSC-derived cardiomyocytes were inoculated with SARS-CoV-2 (MOI 0.1) and analyzed for viability (Zombie-Violet) and infection (NeonGreen) as a function of time by flow cytometry. **Right plot** shows viability of NeonGreen-positive cells ($n = 4$ per group). **(A–D)** Mean values are plotted and error bars denote standard error of the mean. **(E)** Brightfield microscopy showing cytopathic effect in hPSC-derived cardiomyocytes infected with SARS-CoV-2 (MOI 0.1). Representative images from 5 individual samples. **(F)** Flow cytometry of 2-dimensional tissues containing CM and Fb (**left**) or CM, Fb, and Mac (**right**) harvested on day 3 following mock infection or inoculation with SARS-CoV-2 (MOI 0.1). Representative plot from 4 independent samples. Cardiomyocytes (CD90-CD14-) showed prominent NeonGreen fluorescence (**green overlay**). NeonGreen signal was not detected in fibroblasts (CD90+CD14-) or macrophages (CD90-CD14+). **(G)** Quantification of NeonGreen-positive cells from 2-dimensional tissues containing hPSC-cardiomyocytes and fibroblasts or hPSC-cardiomyocytes, fibroblasts, and macrophages ($n = 4$ per group). Bars denotes median value. *$p < 0.05$ compared to mock infection (Mann-Whitney test). **(H)** Transmission electron microscopy micrographs of cardiomyocytes in 2-dimensional tissues infected with either mock or SARS-CoV-2 (MOI 0.1). Tissues were harvested on day 3 post-inoculation. Viral budding (**blue arrow**) and endosomal compartments filled with virions (**black arrow**) are denoted. Scale bars in insets are 100 nm. Representative image from 4 independent samples. FFU = focus forming units; other abbreviation as in **Figure 1**.

FIGURE 3 **RNA Sequencing Identified Viral Transcription and Activation of Innate Immune Response in hPSC-Derived Cardiomyocytes and Tissues**

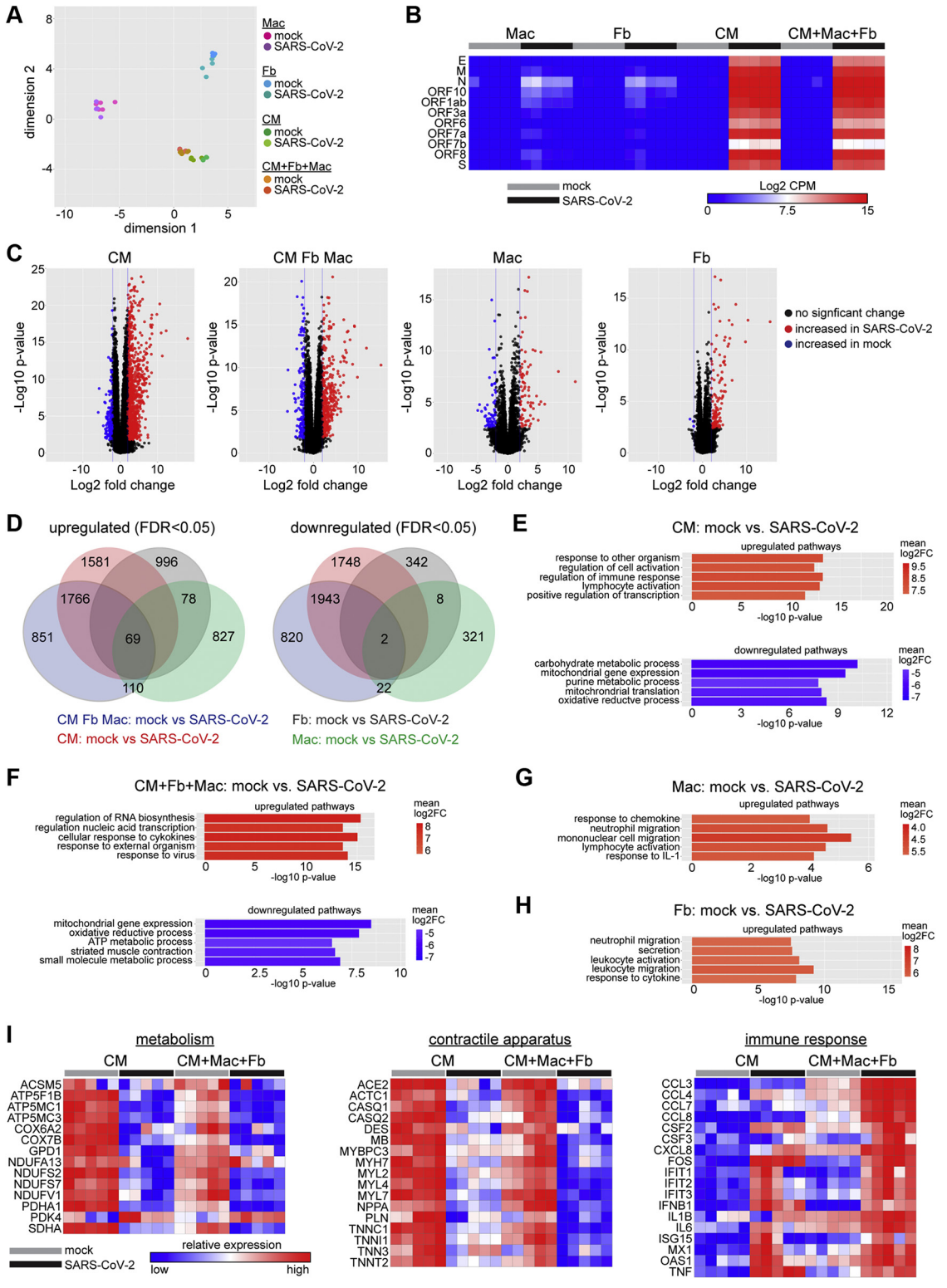

Continued on the next page

$CD90^-CD14^-TNNT2^+$ cardiomyocytes. NeonGreen was not detected in $CD90^+$ fibroblasts or $CD14^+$ macrophages (**Figures 2F, 2G and** Supplemental Figure 6). Transmission electron microscopy of 2-dimensional tissues performed 3 days post-inoculation showed the presence of coronavirus particles within infected hPSC-derived cardiomyocytes. Micrographs revealed structural features of coronaviruses including the presence of a trilaminar envelope and characteristic cross-sections through the nucleocapsid (**Figure 2H**) (21,22). Virions were identified within perinuclear endosomal-like structures of hPSC-derived cardiomyocytes. We observed various stages of virion assembly including budding from intracellular membranes. Virions were not detected in mock-infected cardiomyocytes.

RNA SEQUENCING IDENTIFIED ROBUST VIRAL TRANSCRIPTION AND ACTIVATION OF INNATE IMMUNE RESPONSES. To examine viral transcription and the host immune response to SARS-CoV-2 infection, we performed RNA sequencing. Cultures containing either hPSC-derived cardiomyocytes, fibroblasts, or macrophages were either mock-infected or inoculated with SARS-CoV-2. We also examined 2-dimensional tissues assembled with 80% cardiomyocytes, 10% fibroblasts, and 10% macrophages. Cells and tissues were harvested on day 3 post-inoculation. Multidimensionality reduction analysis revealed separation between experimental groups consistent with their distinct cellular composition (**Figure 3A**). Infected hPSC-derived cardiomyocytes and 2-dimensional tissues contained abundant viral genomic and subgenomic RNAs identified based on the presence of 5' leader sequences (**Figure 3B and** Supplemental Figure 7) (23).

Numerous host genes were differentially regulated upon SARS-CoV-2 infection in each of the examined cell types and 2-dimensional tissues (**Figure 3C**). Conditions that supported viral replication (hPSC-derived cardiomyocytes and 2-dimensional tissues) displayed the greatest overlap in differentially expressed genes. Cell types that did not support viral replication (fibroblasts and macrophages) also showed differentially expressed host genes (**Figure 3D**), suggesting that SARS-CoV-2 virions stimulate host gene expression in the absence of direct viral infection. Pathway analysis revealed that infected hPSC-derived cardiomyocytes and 2-dimensional co-culture tissues showed upregulation of genes associated with immune cell activation, stress-induced transcription, and responses to viral pathogens. Genes associated with muscle contraction, metabolism, oxidative phosphorylation, and mitochondrial function were downregulated (**Figures 3E and 3F**). Host genes differentially expressed in macrophages and fibroblasts were associated with pathways involved in innate immune cell activation, migration, and cytokine responses (**Figures 3G and 3H**).

Specific genes downregulated in infected hPSC-derived cardiomyocytes and 2-dimensional tissues (**Figure 3I**) included components of the electron transport chain (adenosine triphosphate synthase, mitochondrial cytochrome C oxidase, and nicotinamide adenine dinucleotide phosphate dehydrogenase) and metabolic enzymes (glycerol-3-phosphate dehydrogenase, pyruvate dehydrogenase, and succinate dehydrogenase complex). *PDK4*, an inhibitor of pyruvate dehydrogenase, was upregulated in infected hPSC-derived cardiomyocytes and 2-dimensional tissues. Components of the contractile apparatus including cardiac actin, troponins, myosin light and heavy chains, desmin, phospholamban, and calsequestrin were downregulated in infected 2-dimensional tissues. *ACE2* expression was diminished in infected cardiomyocytes and 2-dimensional tissues. Infected hPSC-derived cardiomyocytes and 2-dimensional tissues displayed upregulation of innate immune mediators including *IFNB1* and interferon (IFN)- stimulated genes (*IFIT1*, *IFIT2*, *IFIT3*, *ISG15*, *MX1*, and *OAS1*), early response genes

FIGURE 3 Continued

(A) MDS plot of RNA sequencing data obtained from mock and SARS-CoV-2–infected (MOI 0.1) hPSC-derived CMs, Fbs, Macs, and 2-dimensional tissues (CM + Fb + Mac). Cells and tissues were harvested on day 3 post-inoculation (n = 5 per group). **(B)** Heatmap of SARS-CoV-2 viral gene expression. Color scale denotes absolute expression as log2 counts per million reads (CPM) (scale: **blue** = 0, **red** = 15). **(C)** Volcano plots showing differentially expressed genes between mock and SARS-CoV-2–infected conditions. **Black dots** indicate no significant change, **red dots** indicate upregulated during infection (log2 fold change>2, FDR $p < 0.05$), and **blue dots** indicate downregulated during infection (log2 fold change<2, FDR $p < 0.05$). Data points correspond to individual transcripts. **(D)** Venn diagram of genes upregulated and downregulated in each cell type and tissues. Differential expression is based on change relative to corresponding uninfected (mock) samples. **(E to H)** Gene ontology (GO) pathway analysis of CM **(E)**, CM + Fb + Mac **(F)**, Mac **(G)** and Fib **(H)** showing top 5 upregulated **(red)** and downregulated **(blue)** pathways in SARS-CoV-2–infected samples compared to mock. Color indicates log2 fold change (log2FC). **(I)** Heat maps of selected differentially expressed genes implicated in metabolism **(left)**, contractile apparatus **(center)**, and immune response **(right)**. CM and tissues (CM + Mac + Fb) are displayed. Color scale denotes relative gene expression (high **red**, low **blue**) across cell types and conditions. ATP = adenosine triphosphate; FDR = false discovery rate; IL = interleukin. other abbreviations as in **Figures 1 and 2**.

FIGURE 4 EHTs Recapitulate Aspects of COVID-19 Myocarditis

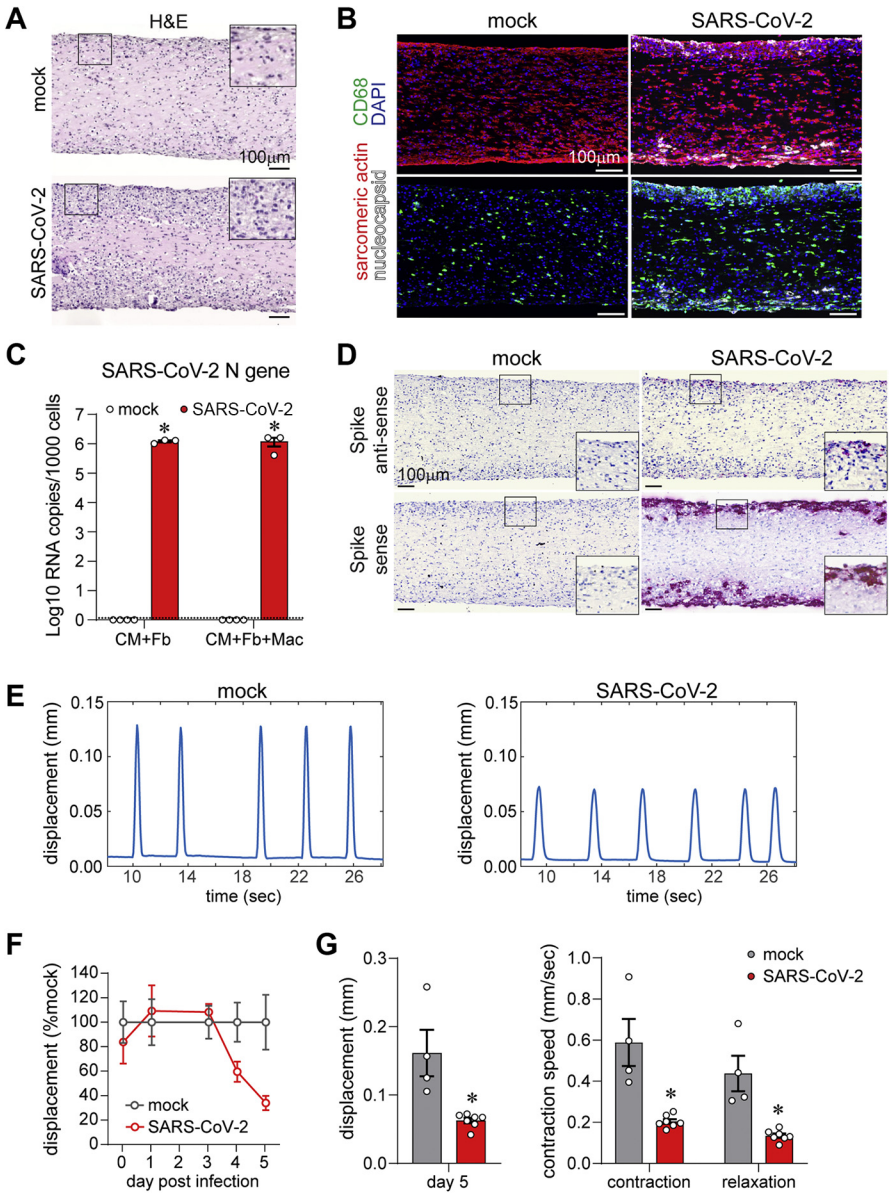

(A) Hematoxylin and eosin (H&E)–stained sections of 3-dimensional engineered heart tissue (EHT) consisting of hPSC-derived CM, Fbs, and Macs 5 days following mock infection or inoculation with SARS-CoV-2 (MOI 0.1). Insets are high-magnification images of the boxed areas. Representative images from 4 independent samples. **(B)** Immunostaining of mock or SARS-CoV-2–infected 3-dimensional EHTs for sarcomeric actin (cardiomyocytes, **red**), CD68 (macrophages, **green**), and nucleocapsid protein **(white)**. EHTs were harvested 5 days post-inoculation. **Blue**: DAPI. Representative images from 4 independent samples. **(C)** Quantitative RT-PCR of SARS-CoV-2 N-gene expression in EHTs consisting of hPSC-derived CM, Fb, and/or Macs. EHTs were either mock infected or inoculated with SARS-CoV-2 (MOI 0.1) and harvested 5 days post-inoculation. **Error bars** denote SE of the mean. **Dotted line:** limit of detection. *$p < 0.05$ compared to uninfected control (mock, Student *t* test test). **(D)** In situ hybridization for SARS-CoV-2 spike RNA sense and antisense strands **(red)** in EHTs 5 days after mock or SARS-CoV-2 infection (MOI 0.1). **Blue**: hematoxylin. Representative images from 4 independent specimens. Insets are high magnification images of the boxed areas. **(E)** Spontaneous beating displacement traces for infected and uninfected EHTs on day 5 post-infection. **(F)** Displacement (relative to uninfected mock condition) generated by spontaneous beating of EHTs as a function of time following inoculation with SARS-CoV-2 (MOI 0.1). Each data point represents a mean value from 4 to 7 independent samples, **error bars** denote SE of the mean. **(G)** Quantification of absolute displacement **(left)** and contraction speed **(right)** generated by spontaneous beating of EHTs 5 days following mock or SARS-CoV-2 infection (MOI 0.1). **Error bars** represent SE of the mean; *$p < 0.05$ compared to mock (Student's *t*-test test). Abbreviations as in Figures 1 and 2.

FIGURE 5 Mechanisms of Reduced EHT Contractility

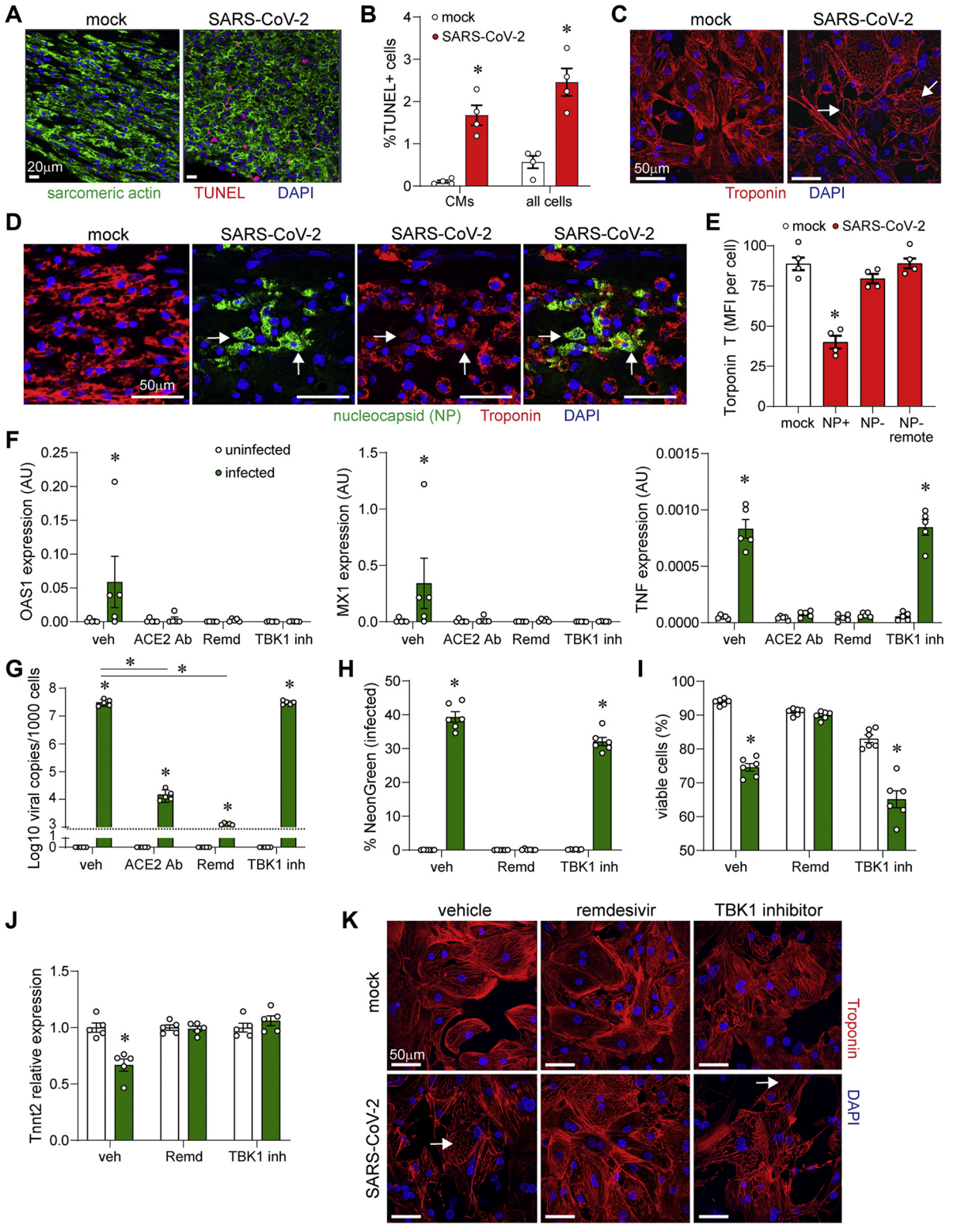

Continued on the next page

(*FOS*), and cytokines (*TNF*). Consistent with a greater innate immune response in 2-dimensional tissues, several chemokines (*CCL3*, *CCL4*, *CCL7*, *CCL8*, and *CXCL8*) and cytokines (*IL1B*, *IL6*, and *CSF3*) were selectively upregulated in infected 2-dimensional tissues. Macrophages and fibroblasts contributed to enhanced chemokine and cytokine expression in 2-dimensional tissues. *CCL3*, *CCL4*, and *CCL8* were selectively expressed in infected macrophages and *CSF3*, *CXCL8*, *IL1B*, and *IL6* were induced in infected fibroblasts (Supplemental Figure 7).

SARS-CoV-2 ENTRY INTO CARDIOMYOCYTES IS MEDIATED BY ACE2 AND ENDOSOMAL CYSTEINE PROTEASES. A neutralizing human ACE2 (viral receptor) antibody abrogated SARS-CoV-2–NeonGreen infectivity as measured by NeonGreen-positivity and viral RNA extracted from the supernatant of infected cultures. The extent of blockade was comparable to treatment with remdesivir, a potent inhibitor of the SARS-CoV-2 RNA-dependent RNA polymerase (24–26) (Supplemental Figure 8). After binding to ACE2, the spike protein must undergo proteolytic activation to initiate membrane fusion (27). Host proteases located at the plasma membrane (TMPRSS2) or within endosomes (cathepsins) most commonly perform this function. The relative contributions of each of these protease families to SARS-CoV-2 infection varies by cell type (17,27). hPSC-derived cardiomyocytes express multiple endosomal proteases including cathepsins and calpains. Low levels of transmembrane protease, serene 2 (TMPRSS2) mRNA were detected in hPSC-derived cardiomyocytes, but not in fibroblasts or macrophages (Supplemental Figure 8). To determine whether SARS-CoV-2 enters cardiomyocytes through an endosomal or plasma membrane route, we inoculated hPSC-derived cardiomyocytes with SARS-CoV-2–NeonGreen and administered either the endosomal cysteine protease inhibitor E-64, which blocks cathepsins, or the serine protease inhibitor camostat mesylate, which blocks TMPRSS2 (and possibly TMPRSS4) (27). E-64 abolished SARS-CoV-2 infection of hPSC-derived cardiomyocytes as shown by reduced NeonGreen expression and viral RNA within the supernatant. Camostat had no effect on cardiomyocyte infection over a range of doses that significantly affect SARS-CoV-2 infection of lung-derived cell lines where TMPRSS2 mediates viral entry (17). Laboratory cultivated SARS-CoV-2 stocks have acquired a mutation in the furin cleavage site, which alters the preference for proteases (TMPRSS2 vs. cathepsins) that mediate SARS-CoV-2 entry (27–29). To assess the impact this mutation on cardiomyocyte infectivity and entry, we inoculated hPSC-derived cardiomyocytes with either wild-type SARS-CoV-2 or recombinant SARS-CoV-2 containing the furin cleavage site mutation (ΔPRRA). Both viruses readily infected cardiomyocytes through an endosomal-dependent mechanism (Supplemental Figure 8).

EHT MODEL COVID-19 MYOCARDITIS. To examine whether SARS-CoV-2 infection of EHTs mimics aspects of COVID-19 myocarditis, we generated EHTs containing hPSC-derived cardiomyocytes, fibroblasts, and macrophages. EHTs were seeded in a collagen-

FIGURE 5 Continued

(A) Terminal deoxynucleotidyl transferase dUTP nick end labelling (TUNEL) stain (**red**) and cardiac actin (**green**) immunostaining of EHTs (CM +Fb + Mac) 5 days after mock or SARS-CoV-2 infection (MOI 0.1). **Blue:** DAPI. Representative images from 4 independent experiments. **(B)** Quantification of TUNEL-positive cells in areas of viral infection. **Error bars** represent SE of the mean, *p < 0.05 compared to mock (Student *t* test). **(C)** Immunostaining of hPSC-derived cardiomyocytes for troponin T (red) 3 days after inoculation with mock control or SARS-CoV-2–NeonGreen (MOI 0.1). **Blue**: DAPI. Arrows denote areas of sarcomere disassembly. **(D)** Immunostaining of EHTs for troponin T (**red**) and SARS-CoV-2 nucleocapsid (**green**) 5 days after inoculation with mock control or SARS-CoV-2–NeonGreen (MOI 0.1). **Blue:** DAPI. Arrows denote SARS-CoV-2 nucleocapsid-positive cells with reduced troponin T staining. **(E)** Quantification of troponin T staining in mock (**white**) and SARS-CoV-2 infected (**red**) EHTs. Data is presented as mean florescence intensity (MFI). MFI was measured in infected (nucleocapsid-positive [NP+]) cardiomyocytes and uninfected (NP-) cardiomyocytes located proximal or remote to areas of infection. **Error bars** represent SE of the mean, *p < 0.05 compared to mock (Student *t* test). **(F)** Quantitative RT-PCR measuring OAS1, MX1, and tumor necrosis factor (TNF) mRNA expression in hPSC-derived cardiomyocytes 3 days post-inoculation with mock control (**white**) or SARS-CoV-2 (**green**, MOI 0.1). Cells were treated with vehicle, angiotensin-converting enzyme 2 antibody (ACE2 Ab) (20 μg/ml), remdesivir (10 μM), or TBK inhibitor (MRT67307, 10μM). **Error bars** indicate SE of the mean. *p < 0.05 compared to mock control (Student *t* test). **(G)** Quantitative RT-PCR of SARS-CoV-2 N gene expression in hPSC-derived cardiomyocytes that were either mock infected (**white**) or inoculated with SARS-CoV-2 (**green**, MOI 0.1) and harvested 3 days post-inoculation. **Error bars** denote SE of the mean. **Dotted line:** limit of detection. *p < 0.05 compared to uninfected control (analysis of variance [ANOVA]) or vehicle infected as indicated by the bar (ANOVA). **(H,I)** Flow cytometry measuring the percent of infected (**H**) and viable (**I**) cardiomyocytes following either mock infection (**white**) or inoculation with SARS-CoV-2 (**green**, MOI 0.1). Cells were harvested and analyzed 3 days post-inoculation. **Error bars** denote SE of the mean. *p < 0.05 compared to uninfected control (ANOVA). **(J)** Quantitative RT-PCR measuring TNNT2 mRNA expression 3 days post-inoculation with mock control (**white**) or SARS-CoV-2 (**green**, MOI 0.1). **Error bars** indicate SE of the mean. *p < 0.05 compared to mock control (ANOVA). **(K)** Immunostaining for troponin T (**red**) 3 days post-inoculation with mock control or SARS-CoV-2–NeonGreen (MOI 0.1). **Blue:** DAPI. **Arrows** denote areas of sarcomere disassembly. Abbreviations as in **Figures 1 and 2**.

Matrigel matrix between 2 PDMS posts, infected with SARS-CoV-2, and harvested 5 days after inoculation. Hematoxylin and eosin staining revealed increased interstitial cell abundance within the periphery of SARS-CoV-2-infected EHTs (**Figure 4A**). Immunostaining for the viral nucleocapsid protein demonstrated evidence of infected cardiomyocytes at the periphery of the tissue, possible representing limited diffusion of the virus in the EHT environment. CD68 immunostaining showed macrophage accumulation corresponding to sites of viral infection (**Figure 4B,** Supplemental Figure 9). Infected EHTs accumulated high levels of viral RNA (**Figure 4C**). In situ hybridization for viral spike sense and antisense RNA indicated active viral replication within EHTs (**Figure 4D**) (Supplemental Figure 10).

As reduced LV systolic function has been reported in severe cases of COVID-19 myocarditis, we examined the effect of SARS-CoV-2 infection on EHT contractility (30). We calculated the average peak displacement and velocity for each spontaneously contracting tissue (Videos 1 and 2). EHTs consisting of hPSC-derived cardiomyocytes and fibroblasts were inoculated with SARS-CoV-2, and contractile function analyzed daily. SARS-CoV-2-inoculated tissues showed reduced contraction, speed of contraction, and relaxation relative to the mock-infected tissues (**Figures 4E to 4G**).

To examine whether cardiomyocyte cell death might serve as a mechanism explaining reduced EHT contractility, we performed terminal deoxynucleotidyl transferase dUTP nick end labelling (TUNEL) staining and observed increased numbers of TUNEL-positive cardiomyocytes in SARS-CoV-2-infected EHTs on day 5 post infection (**Figures 5A and 5B**). Our RNA sequencing data suggested that other mechanisms also may contribute to reduced EHT contractility, including sarcomere structure, metabolism, and/or host immune responses (**Figure 3I**). Immunostaining of hPSC-derived cardiomyocytes infected with SARS-CoV-2 revealed evidence of sarcomere loss 3 days following infection (**Figure 5C**), a time point that preceded cell death. Immunostaining of EHTs showed reduced troponin T expression in infected cardiomyocytes (**Figures 5D and 5E**).

We then examined the mechanistic relationship between cardiomyocyte infection, inflammatory signaling, sarcomere loss, and cell death. Inhibition of viral entry (ACE2 neutralizing antibody) or viral replication (remdesivir) was sufficient to prevent type I IFN and tumor necrosis factor (TNF) expression following SARS-CoV-2 infection (**Figures 5F and 5G**). Remdesivir similarly reduced inflammatory gene expression in 3-dimensioinal EHTs (Supplemental Figure 11), establishing that viral infection represents the upstream driver of inflammation in our model system.

To examine the impact of cardiomyocyte inflammatory signaling on cell death, sarcomere gene expression, and sarcomere structure, we focused on inhibiting viral nucleic acid sensing in 2-dimensional cultures given their amenability to flow cytometry and high-resolution imaging. TANK-binding kinase 1 (TBK1) is an essential mediator of nucleic acid sensing pathways including RIG-I, MAVS, STING, and TLRs (31,32). Inhibition of TBK1 activity reduced type I IFN activity (inflammatory signature in infected cardiomyocytes) (**Figure 3I**) without impacting viral load, cardiomyocyte infectivity, or cell death (**Figures 5F to 5I**). While TBK1 inhibition prevented reductions in TNNT2 and MYH7 mRNA expression following SARS-CoV-2 infection, sarcomere breakdown remained prevalent. In contrast, remdesivir prevented both reductions in TNNT2 and MYH7 mRNA expression and sarcomere loss following SARS-CoV-2 infection (**Figures 5J, 5K, and** Supplemental Figure 11). These data indicate that sarcomeric disassembly and cardiomyocyte cell death are the result of cardiomyocyte infection and not inflammation in the EHT system.

DISCUSSION

Whether cardiac manifestations of COVID-19 are a result of viral infection, systemic inflammation, and/or microvascular thrombosis remains a debated topic. We examined myocardial specimens obtained from individuals with severe COVID-19 myocarditis and revealed evidence of cardiomyocyte infection, cell death, and macrophage infiltration. These findings are consistent with prior reports highlighting infiltration of monocytes, lymphocytes, and plasma cells in an endomyocardial biopsy specimen from a patient with suspected COVID-19 myocarditis and viral RNA within the myocardium of COVID-19 autopsy specimens (33,34). The specimens examined in this study differ substantially from published autopsy series, which did not include subjects with cardiac manifestations (3,35). Here, we exclusively focused on subjects with COVID-19 infection and severe myocarditis based on echocardiography and clinical presentation.

We further provide evidence that SARS-CoV-2 infects and replicates within human cardiomyocytes. SARS-CoV-2 was unable to replicate in cardiac

fibroblasts, endothelial cells, and macrophages. It remains possible that SARS-CoV-2 could also infect other cardiac cell types that are difficult to isolate from the human heart such as pericytes and endocardial cells. Despite these limitations, our findings clearly show that cardiomyocytes are a target of SARS-CoV-2 infection.

To gain insights into the mechanistic basis of cardiomyocyte infection and myocarditis, we developed a human EHT system that recapitulates features of SARS-CoV-2-induced myocarditis. We provide evidence that SARS-CoV-2 infects hPSC-derived cardiomyocytes, resulting in reduced metabolic and contractile apparatus gene expression, sarcomeric disassembly, inflammatory signaling, and cell death. Viral entry was ACE2-dependent and relied on endosomal cysteine protease activity. Our findings are consistent with a recent report suggesting that SARS-CoV-2 infects human cardiac slices, hPSC-derived cardiomyocytes in an ACE2 and cathepsin-dependent manner, and impacts the beating of cardiospheres (36). We extend these observations to show that cardiomyocytes supported viral replication, rapidly produced infectious virions, activated type I IFN signaling, and displayed cytopathic features seen with coronavirus infection. Infected EHTs showed reduced contractile force, sarcomere disassembly, and pathological evidence of myocarditis including macrophage activation.

Extrapulmonary cell types are susceptible to SARS-CoV-2 infection (37–39). This broader cellular tropism is dictated by ACE2 expression and the ability of the virus to gain access to extrapulmonary tissues. Whether SARS-CoV-2 enters the heart through hematological seeding and/or direct extension from the pleural cavity remains unknown. Among myocardial cell types, cardiomyocytes and pericytes express ACE2 mRNA (19). Cardiac fibroblasts and vascular smooth muscle cells may also express ACE2 (20). We showed that ACE2 is preferentially expressed in cardiomyocytes and is essential for SARS-CoV-2 to infect cardiomyocytes. It remains to be explored whether cardiomyocyte maturation or remodeling impact vulnerability to viral infection. This possibility is supported by the heterogeneous expression of ACE2 in the human heart and may explain why pre-existing cardiovascular disease represents a strong risk factor for COVID-19 mortality. Consistent with this idea, ACE2 expression is increased in heart failure (30,40).

EHTs provided an opportunity to gain insights into the relationship between cardiomyocyte infection, myocardial inflammation, and contractile dysfunction. Infection of EHTs resulted in inflammatory mediator generation, decreased ACE2 expression, cardiomyocyte cell death, sarcomere breakdown, and reduced sarcomeric and metabolic gene expression. Each of these mechanisms likely contributes to diminished EHT contractility. We showed that cardiomyocyte infection triggers inflammatory gene expression, sarcomere loss, and cell death. Blockade of viral nucleic acid sensing pathways did not prevent sarcomere disassembly or cardiomyocyte cell death. Despite the limitations of the inherent immaturity of hPSC-derived cardiomyocytes and incomplete representation of human myocardial cell types included in EHTs, these findings highlight the central role of cardiomyocyte infection and suggest that targeting viral cell entry, replication, or sarcomere breakdown may improve outcomes in patients with cardiac complications of COVID-19. The relevance of ACE2 downregulation in infected cardiomyocytes will require further clarification as *Ace2*$^{-/-}$ mice display LV systolic dysfunction and heart failure (41).

STUDY LIMITATIONS. While our findings implicate that SARS-CoV-2 cardiomyocyte infection likely contributes to myocardial dysfunction, our findings do not exclude an important role for inflammation or microthrombi in COVID-19 cardiac pathology. Macrophages and fibroblasts likely contribute to the inflammatory response. Despite resistance to SARS-CoV-2 infection, macrophages and fibroblasts generated inflammatory mediators when exposed to SARS-CoV-2. This response could be a result of direct recognition of viral RNAs and proteins or communication with infected cardiomyocytes through production of soluble mediators or intercellular transfer via gap junctions. Future studies are necessary to dissect the cellular mechanisms and signaling pathways that initiate and convey the adverse impact of myocardial inflammation.

CONCLUSIONS

This study provides evidence that cardiomyocytes are a target of SARS-CoV-2 in the human heart and support the conclusion that SARS-CoV-2 infection of cardiomyocytes and resultant myocardial injury and inflammation contribute to the cardiac manifestations of COVID-19. We show that SARS-CoV-2 infection of 2-dimensional cultures and EHTs results in reductions in cardiac contractility through

sarcomere breakdown, disruption of metabolic gene expression, and cardiomyocyte death. Collectively, these findings show that SARS-CoV-2 can productively infect human cardiomyocytes and establish an experimentally tractable platform for mechanistic and therapeutic investigation of COVID-19 myocardial pathology.

ACKNOWLEDGMENTS The authors thank Dr. Cynthia Goldsmith for help interpreting electron microscopy micrographs and the McDonnell Genome Institute (MGI) at Washington University School of Medicine for assistance in performing sequencing and analysis.

FUNDING SUPPORT AND AUTHOR DISCLOSURES

Supported by the National Institutes of Health (R01 HL141086 to Dr. M.J. Greenberg; R01 HL138466, and R01 HL139714 to Dr. Lavine; 75N93019C00062, and R01 AI127828 to Dr. Diamond); Burroughs Welcome Fund (1014782 to Dr. Lavine); Defense Advanced Research Project Agency (HR001117S0019 to Dr. Diamond); the March of Dimes Foundation (FY18-BOC-430198 to Dr. M.J. Greenberg.); Foundation of Barnes-Jewish Hospital (8038-88 to Dr. Lavine.); and Children's Discovery Institute of Washington University and St. Louis Children's Hospital (CH-II-2017-628 to Dr. Lavine; PM-LI-2019-829 to Drs. Lavine and M.J. Greenberg.). Imaging was performed in the Washington University Center for Cellular Imaging (WUCCI) which is funded, in part by the Children's Discovery Institute of Washington University and St. Louis Children's Hospital (CDI-CORE-2015-505, CDI-CORE-2019-813) and the Foundation for Barnes-Jewish Hospital (3770). Dr. Diamond is a consultant for Inbios, Eli Lilly, Vir Biotechnology, NGM Biopharmaceuticals; is a member of the Scientific Advisory Board of Moderna; and has received funding and unrelated sponsored research agreements from Moderna, Vir Biotechnology, and Emergent BioSolutions. Dr. Lavine is a member of the Medtronic: DT-PAS/APOGEE trial advisory board; and has received funding and unrelated sponsored research agreements from Amgen. All other authors have reported that they have no relationships relevant to the contents of this paper to disclose.

ADDRESS FOR CORRESPONDENCE: Dr. Kory J. Lavine, Department of Pathology and Immunology, Washington University School of Medicine, 660 South Euclid Campus Box 8086, St. Louis, Missouri 63110, USA. E-mail: klavine@wustl.edu.

PERSPECTIVES

COMPETENCY IN MEDICAL KNOWLEDGE: Defining viral tropism is fundamental to understanding the pathogenesis of infective myocarditis and associated heart failure. Improved knowledge regarding the myocardial cell types impacted by SARS-CoV-2, mechanisms of cell entry, and outcomes of infected cells will yield information needed to understand, model, and device treatments for COVID-19–associated cardiac pathology.

TRANSLATIONAL OUTLOOK: Engineered heart tissues provide an experimentally tractable human model of COVID-19 myocarditis and cardiac pathology. Future studies leveraging this platform may provide mechanistic insights regarding the lifecycle of SARS-CoV-2 in cardiomyocytes, mechanisms of sarcomere breakdown, cell death, and immune cell activation. Such observations may inform the use and development of therapeutics for cardiac manifestations of COVID-19.

REFERENCES

1. Madjid M, Safavi-Naeini P, Solomon SD, Vardeny O. Potential effects of coronaviruses on the cardiovascular system: a review. JAMA Cardiol 2020;5:831–40.

2. Zhou F, Yu T, Du R, et al. Clinical course and risk factors for mortality of adult inpatients with COVID-19 in Wuhan, China: a retrospective cohort study. Lancet 2020;395:1054–62.

3. Shi S, Qin M, Shen B, et al. Association of cardiac injury with mortality in hospitalized patients with COVID-19 in Wuhan, China. JAMA Cardiol 2020;5:802–10.

4. Bhatla A, Mayer MM, Adusumalli S, et al. COVID-19 and Cardiac Arrhythmias. Heart Rhythm 2020;17:1439–44.

5. Huang L, Zhao P, Tang D, et al. Cardiac Involvement in Patients Recovered From COVID-2019 Identified Using Magnetic Resonance Imaging. J Am Coll Cardiol Img 2020;13:2330–9.

6. Puntmann VO, Carerj ML, Wieters I, et al. Outcomes of cardiovascular magnetic resonance imaging in patients recently recovered from coronavirus disease 2019 (COVID-19). JAMA Cardiol 2020;5:1265–73.

7. Rajpal S, Tong MS, Borchers J, et al. Cardiovascular magnetic resonance findings in competitive athletes recovering from COVID-19 infection. JAMA Cardiol 2020;6:116–8.

8. Tersalvi G, Vicenzi M, Calabretta D, Biasco L, Pedrazzini G, Winterton D. Elevated troponin in patients with coronavirus disease 2019: possible mechanisms. J Card Fail 2020;26:470–5.

9. Cleary SJ, Pitchford SC, Amison RT, et al. Animal models of mechanisms of SARS-CoV-2 infection and COVID-19 pathology. Br J Pharmacol 2020;177:4851–65.

10. Letko M, Marzi A, Munster V. Functional assessment of cell entry and receptor usage for SARS-CoV-2 and other lineage B betacoronaviruses. Nat. Microbiol 2020;5:562–9.

11. Wan Y, Shang J, Graham R, Baric RS, Li F. Receptor recognition by the novel coronavirus from Wuhan: an analysis based on decade-long structural studies of SARS coronavirus. J Virol 2020;94:e00127.

12. Abe M, Oshima RG. A single human keratin 18 gene is expressed in diverse epithelial cells of transgenic mice. J Cell Biol 1990;111:1197–206.

13. Xie X, Muruato A, Lokugamage KG, et al. An Infectious cDNA clone of SARS-CoV-2. Cell Host Microbe 2020;27:841–8.e3.

14. Michaud K, Basso C, d'Amati G, et al. Diagnosis of myocardial infarction at autopsy: AECVP reappraisal in the light of the current clinical classification. Virchows Arch 2020;476:179–94.

15. Sabatasso S, Mangin P, Fracasso T, Moretti M, Docquier M, Djonov V. Early markers for myocardial ischemia and sudden cardiac death. Int J Legal Med 2016;130:1265–80.

16. Aljakna A, Lauer E, Lenglet S, et al. Multiplex quantitative imaging of human myocardial infarction by mass spectrometry-immunohistochemistry. Int J Legal Med 2018;132:1675–84.

17. Hoffmann M, Kleine-Weber H, Schroeder S, et al. SARS-CoV-2 cell entry depends on ACE2 and

TMPRSS2 and is blocked by a clinically proven protease inhibitor. Cell 2020;181:271–80.e8.

18. Bao L, Deng W, Huang B, et al. The pathogenicity of SARS-CoV-2 in hACE2 transgenic mice. Nature 2020;583:830–3.

19. Chen L, Li X, Chen M, Feng Y, Xiong C. The ACE2 expression in human heart indicates new potential mechanism of heart injury among patients infected with SARS-CoV-2. Cardiovasc Res 2020;116:1097–100.

20. Tucker NR, Chaffin M, Bedi KC, et al. Myocyte-specific upregulation of ACE2 in cardiovascular disease: implications for SARS-CoV-2–mediated myocarditis. Circulation 2020;142:708–10.

21. Goldsmith CS, Tatti KM, Ksiazek TG, et al. Ultrastructural characterization of SARS coronavirus. Emerg Infect Dis 2004;10:320–6.

22. Goldsmith CS, Miller SE, Martines RB, Bullock HA, Zaki SR. Electron microscopy of SARS-CoV-2: a challenging task. Lancet 2020;395:e99.

23. Kim D, Lee J-Y, Yang J-S, Kim JW, Kim VN, Chang H. The architecture of SARS-CoV-2 transcriptome. Cell 2020;181:914–21.e10.

24. Gordon CJ, Tchesnokov EP, Woolner E, et al. Remdesivir is a direct-acting antiviral that inhibits RNA-dependent RNA polymerase from severe acute respiratory syndrome coronavirus 2 with high potency. J Biol Chem 2020;295:6785–97.

25. Yin W, Mao C, Luan X, et al. Structural basis for inhibition of the RNA-dependent RNA polymerase from SARS-CoV-2 by remdesivir. Science 2020;368:1499–504.

26. Agostini ML, Andres EL, Sims AC, et al. Coronavirus susceptibility to the antiviral remdesivir (GS-5734) is mediated by the viral polymerase and the proofreading exoribonuclease. mBio 2018;9:e0021–118.

27. Simmons G, Zmora P, Gierer S, Heurich A, Pöhlmann S. Proteolytic activation of the SARS-coronavirus spike protein: cutting enzymes at the cutting edge of antiviral research. Antiviral Res 2013;100:605–14.

28. Hoffmann M, Kleine-Weber H, Pöhlmann S. A multibasic cleavage site in the spike protein of SARS-CoV-2 is essential for infection of human lung cells. Mol Cell 2020;78:779–84.e5.

29. Johnson BA, Xie X, Kalveram B, et al. Furin cleavage site is key to SARS-CoV-2 pathogenesis. bioRxiv 2020 Aug 26 [Epub ahead of print]. Available at: http://biorxiv.org/lookup/doi/10.1101/2020.08.26.268854. Accessed December 23, 2020.

30. Hu H, Ma F, Wei X, Fang Y. Coronavirus fulminant myocarditis saved with glucocorticoid and human immunoglobulin. Eur Heart J 2021;42:206.

31. Zhou R, Zhang Q, Xu P. TBK1, a central kinase in innate immune sensing of nucleic acids and beyond. Acta Biochim Biophys Sin 2020;52:757–67.

32. Bartok E, Hartmann G. Immune sensing mechanisms that discriminate self from altered self and foreign nucleic acids. Immunity 2020;53:54–77.

33. Tavazzi G, Pellegrini C, Maurelli M, et al. Myocardial localization of coronavirus in COVID-19 cardiogenic shock. Eur J Heart Fail 2020;22:911–5.

34. Puelles VG, Lütgehetmann M, Lindenmeyer MT, et al. Multiorgan and renal tropism of SARS-CoV-2. N Engl J Med 2020;383:590–2.

35. Lindner D, Fitzek A, Bräuninger H, et al. Association of cardiac infection with SARS-CoV-2 in confirmed COVID-19 autopsy cases. JAMA Cardiol 2020;5:1281–5.

36. Bojkova D, Wagner JUG, Shumliakivska M, et al. SARS-CoV-2 infects and induces cytotoxic effects in human cardiomyocytes. Cardiovasc Res 2020;116:2207–15.

37. Lamers MM, Beumer J, van der Vaart J, et al. SARS-CoV-2 productively infects human gut enterocytes. Science 2020;369:50–4.

38. Monteil V, Kwon H, Prado P, et al. Inhibition of SARS-CoV-2 infections in engineered human tissues using clinical-grade soluble human ACE2. Cell 2020;181:905–13.e7.

39. Yang L, Han Y, Nilsson-Payant BE, et al. A human pluripotent stem cell-based platform to study SARS-CoV-2 tropism and model virus infection in human cells and organoids. Cell Stem Cell 2020;27:125–36.e7.

40. Bos JM, Hebl VB, Oberg AL, et al. Marked up-regulation of ACE2 in hearts of patients with obstructive hypertrophic cardiomyopathy: implications for SARS-CoV-2–mediated COVID-19. Mayo Clin Proc 2020;95:1354–68.

41. Crackower MA, Sarao R, Oudit GY, et al. Angiotensin-converting enzyme 2 is an essential regulator of heart function. Nature 2002;417:822–8.

KEY WORDS cardiomyocyte, coronavirus disease 2019, engineered heart tissue, myocarditis, severe acute respiratory syndrome coronavirus 2

APPENDIX For an expanded Methods section as well as supplemental figures, tables, and videos, please see the online version of this paper.